ACS Sustainable Chemistry & Engineering

pubs.acs.org/journal/ascecg

Research Article

Transparent Multifunctional Cellulose Nanocrystal Films Prepared Using Trivalent Metal Ion Exchange for Food Packaging

Cong Chen, Wenjing Sun, Lu Wang, Mehdi Tajvidi, Jinwu Wang,* and Douglas J. Gardner*

Cite This: *ACS Sustainable Chem. Eng.* 2022, 10, 9419−9430

Read Online

ACCESS | Metrics & More | Article Recommendations | Supporting Information

ABSTRACT: To better preserve food from the interaction with oxygen, moisture, and (light) ultraviolet (UV) radiation, typical polymer film packaging is produced as opaque or metalized sheets. There is increasing consumer demand for multifunctional transparent packaging or a transparent window to allow viewing of food before consumer purchase. Cellulose nanocrystals (CNCs), as a type of sustainable and biodegradable material, show great potential for transparent food packaging by providing good oxygen permeation resistance. However, CNCs are poor in preventing UV light transmission, sensitive to water, and too brittle to make flexible films. This work aimed to produce high-quality CNC films with multifunctional properties using a facile processing method. CNC suspensions were modified with different concentrations of trivalent metal ions (Al^{3+} and Fe^{3+}). Homogeneous, transparent, and flexible CNC films were prepared by solvent casting. CNC films underwent cross-linking between metal ions and sulfate half-ester groups of the CNCs, leading to high UV absorption properties. In addition, the water vapor and oxygen transmission rates of the cross-linked films were decreased, and the durability of films in water was improved. The CNC films displayed excellent oil/grease resistance and fire self-extinguishment.

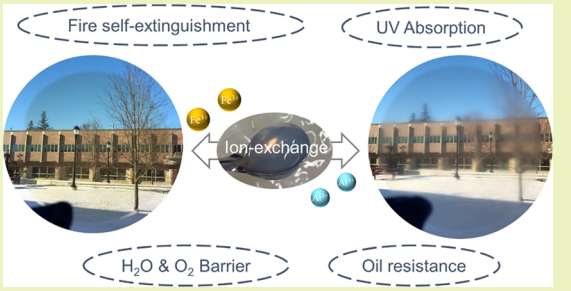

KEYWORDS: *cellulose nanocrystals (CNCs), packaging, barrier properties, trivalent metal ions*

INTRODUCTION

Food packaging provides means to mitigate food spoilage caused by microbes and environmental exposure, as well as prolonging the shelf life of food products in a cost-effective manner that industry and consumers desire while minimizing environmental impact.[1] A variety of materials have been used in the food packaging field, for example, glass, metal, paper, and plastic (Figure 1). Therein, plastic materials derived from petroleum comprise a large proportion of food packaging applications because of their strength, flexibility, lightweight, low-cost, and good processability advantages.[2,3] According to recent reports, 368 million metric tons of plastic materials were produced for the global market in 2019, of which approximately 40% went to packaging uses.[4] Packaging production will continue to grow, projected to exceed 250 million metric tons by 2050.[5] For conventional plastics, polyethylene (PE), polypropylene (PP), and polyethylene terephthalate are the most common types of polymers that are used in packaging applications. However, these unsustainable, nonrenewable, and nondegradable packaging materials can accumulate and cause serious and irreversible pollution to oceans and landfills and even to human health via microplastic particle release.[6] Taking the above issues into consideration, bio-based and biodegradable materials are desirable to address the end-of-life issues for packaging (Figure 1).

Polylactic acid (PLA), polyhydroxyalkanoates, and polybutylene succinate are synthesized from bio-based sources and

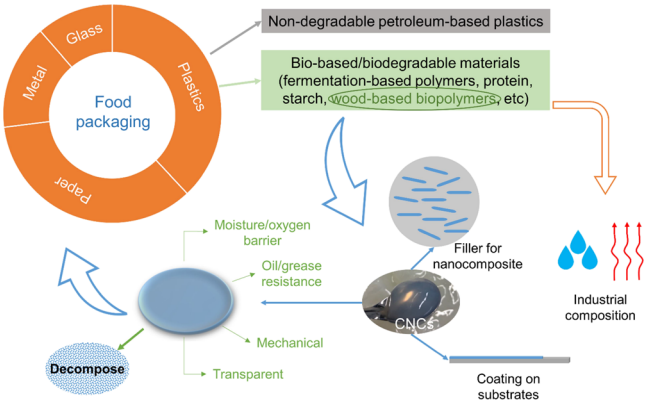

Figure 1. Different materials and required characteristics for food packaging and the great potential of CNCs.

Received: March 26, 2022
Revised: July 1, 2022
Published: July 14, 2022

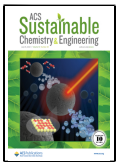

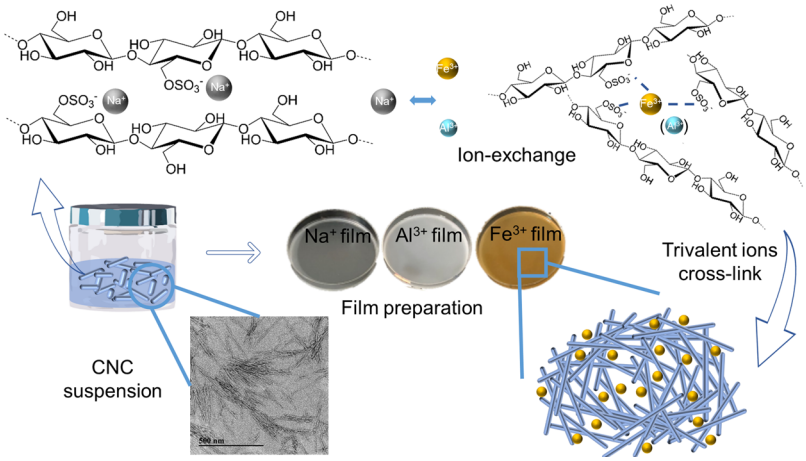

Figure 2. Hypothesized mechanism of ion-exchanged film formation. CNCs are cross-linked by trivalent metal ions.

are produced on an industrial scale currently.[7] The majority of current bio-based polymer materials are neither biodegradable nor home-compostable. They can only decompose under specific temperature and humidity conditions in industrial composting systems.[8] Other kinds of bio-based materials, such as proteins (soy, whey, gluten, and collagen) and polysaccharides (starch, chitosan, and alginate), are also being researched for biodegradable food packaging materials.[9] While most of the food-based materials are also indispensable sources for human consumption, excessive use in materials production could lead to undesirable competition in their utilization. This is problematic, especially in many regions of the world that are facing food shortages.

Consequently, wood-based biomaterials could be regarded as prospective food packaging materials. Cellulose nanomaterials (CNMs), such as cellulose nanofibrils (CNFs) and cellulose nanocrystals (CNCs), are being investigated widely and have tremendous potential in the packaging field as a natural material.[10−14] CNFs are mainly obtained through mechanical shear refinement with >1 μm length and a 10−100 aspect ratio (spaghetti-like structure). For packaging applications, CNF films are usually prepared via a filtration or casting method, exhibiting great mechanical properties (around 110 MPa tensile strength) and barrier properties.[15−17] Nevertheless, some chemical modifications, such as 2,2,6,6-tetramethylpiperidine-1-oxyl radical (TEMPO)-mediated oxidation[18−20] and hot-press treatments, are usually conducted in CNF film fabrication to further improve their properties.[21] The high-energy-consuming procedures and opacity of the resulting CNF films also limit their wide application. CNCs are produced by acid hydrolysis of purified cellulose, where the amorphous regions are degraded, leaving behind the cellulose crystal regions.[22−24] CNCs display excellent performance, like high specific surface area, low density, high mechanical strength arising from their nanoscale dimension,[12] and outstanding transparency. CNCs are mainly considered as a reinforcement filler or components mixed with other matrices to prepare nanocomposite films or coatings on substrates for food packaging applications. CNCs have been reported to be mixed with guar gum, pectin, carrageenan, or PLA to prepare films with great mechanical and barrier properties for food packaging[25−28] and blended with polyvinyl alcohol for coating processes.[29,30] Only very few studies have demonstrated free-standing CNC films for food packaging.[16] However, CNC films are extremely sensitive to moisture or water, and they start to disintegrate immediately when in contact with water. Moreover, a suitable food packaging material should fulfill other requirements, and therefore, moisture or oxygen barrier properties, oil/grease resistance, ultraviolet (UV) protection, and flame retardance should be considered as well (Figure 1). Therefore, appropriate and facile chemical modifications or additives are usually introduced into the CNM film to overcome the above shortcomings. According to previous research, multivalent metal ions as counterions mixed with TEMPO-CNF have been widely demonstrated for versatile applications. Multivalent cations could promote the formation of cross-links among CNFs because the carboxylate groups of TEMPO-CNF have affinity to metal ions, leading to metal−carboxylate complexes.[20,31−33] The counterion on the surface of CNMs can act as an active site and be designed to produce specific material properties. Thus, multivalent metal ions could be introduced into a CNC system without further modification since ionic sulfate half-ester groups are produced by sulfuric acid hydrolysis during CNC preparation. Some studies have reported that multivalent cations could affect the colloidal stabilization of CNCs by clustering or cross-linking.[34−36] Meanwhile, CNCs show economic advantages compared to TEMPO-CNF.[37]

In this study, we developed a facile and effective approach to prepare free-standing CNC films with excellent material properties. There are sulfate half-easter groups formed on the CNC surface during sulfuric acid hydrolysis and Na^+ introduced by sodium hydroxide neutralization. The CNC films were produced by trivalent metal ion-exchanged Na^+ modification accompanied by cross-linking between the metal cations and sulfate groups on the CNC surfaces (Figure 2). Before film casting, CNC suspensions were characterized by transmission electron microscopy (TEM) and rheometry. As for the ion-exchanged CNC films, the physical properties, morphology, UV absorption, barrier, mechanical properties, and fire self-extinguishment were fully described. We believe that this facile, economic, and environmentally friendly approach to producing CNC films creates the potential for the next generation of materials for packaging applications.

MATERIALS AND METHODS

Materials. Aluminum chloride ($AlCl_3$), ferric chloride ($FeCl_3$), and D-sorbitol (>98%) were purchased from Sigma-Aldrich. CNCs in suspension with 10.3 wt% solid content were provided by the USDA

https://doi.org/10.1021/acssuschemeng.2c01805
ACS Sustainable Chem. Eng. 2022, 10, 9419−9430

Table 1. CNC Suspensions Modified with $AlCl_3$ and $FeCl_3$ Solutions

item	molar ratio M^{3+}/OSO_3^-	Na^+ (mmol/kg)	Fe^{3+} (mmol/kg)	Al^{3+} (mmol/kg)
Na^+	original	387		
Fe^{3+}-L	1:3	402	117	
Fe^{3+}-M	1:1	76	244	
Fe^{3+}-H	3:1	53	366	
Al^{3+}-L	1:3	356		123
Al^{3+}-M	1:1	77		175
Al^{3+}-H	3:1	44		273

Forest Products Laboratory (Madison, Wisconsin, USA) and were produced through the sulfuric acid hydrolysis method followed by sodium hydroxide neutralization.[38] Distilled water was used for producing CNC suspensions for film production.

Ion-Exchanged CNC Suspensions and Film Preparation. *CNC Suspension Modification.* Three molar ratios of trivalent ions to sulfate ions were prepared according to Table 1. The amount of $AlCl_3$ or $FeCl_3$ for a specific amount of CNCs can be calculated based on the stoichiometric ratio of the sulfate half-ester group to the metal ion. Specifically, the suspensions containing 29.64 g of CNC suspension were diluted with distilled water to 2 wt% and then mixed with 5, 15, or 45 mM concentrations of aluminum chloride ($AlCl_3$) or ferric chloride ($FeCl_3$) under magnetic stirring for 2 h, respectively, forming new suspensions with M^{3+}/OSO_3^- at 1:3, 1:1, and 3:1, respectively. The samples were denoted as CNC-M-C (where M denotes the metal cation type, and C denotes the ratio of the treatment metal ion to sulfate: L (low)-1:3, M (medium)-1:1, and H (high)-3:1.

CNC Suspension Characterization. The cross-linked CNCs were examined by TEM at an accelerating voltage of 100 kV (Philips CM10). Ion-exchanged or control CNC suspensions were diluted to around 0.1 wt% and dropped on carbon-coated grids, followed by uranyl acetate solution staining. The excess liquid was removed using filter paper, and the samples were dried using a lamp before performing TEM analyses.

Viscosity tests were carried out using a Bohlin Gemini parallel plate (25 mm) rheometer (Malvern Instruments, UK) to measure the cross-linking interactions between sulfate ions and metal ions. The steady-state shear viscosity was measured under a shear ramp mode with shear rates ranging from 0.01 to 100 s^{-1} at 25 °C.

Sulfur Content Determination. The sulfur and sodium ion contents of the CNCs were determined by inductively coupled plasma-optical emission spectrometry (ICP-OES) (iCAP 6300, Thermo Fisher Scientific, USA) according to EPA Method 3050b. The sulfur content associated with the sulfate half-ester group ($-O-SO_3^-$) was 355 mmol/kg. The sodium and trivalent ion contents of ion-exchanged CNC samples were also detected by ICP-OES and are listed in Table 1. More details are described in the Supporting Information.

Ion-Exchanged CNC Film Preparation. After 2 h of magnetic stirring, ion-exchanged CNC suspensions were centrifuged at 5000 rpm and 25 °C for 10 min (Thermo Electron Sorvall RC-6Plus, Waltham, MA, USA). The solids were isolated, washed, and centrifuged three times to remove excess metal ions and chloride ions. The moisture content of the sediments after the third centrifugation was determined with a moisture analyzer (Ohaus MB45, USA). The sediments were diluted to 2 wt%, and a total of 15% D-sorbitol based on the CNC solid weight was added. The CNC suspensions were evenly mixed, cast into 100 mm polystyrene Petri dishes, and dried in a fume hood. Eventually, films with a nominal casting weight of 40 g/m^2 were obtained. Before testing, films were conditioned in a conditioning room at 50% relative humidity (RH) and 23 °C for at least 24 h.

Properties and Characterizations of Films. *Optical Properties of Films.* Color values of the CNC films were measured by color spectrophotometry (Technidyne ColorTouchX, New Albany, IN, USA) with five replications for each sample. Graphs were prepared in OriginPro software 2020 (Chromaticity Diagram app).

Transparency and UV absorption of films were measured using a UV−vis spectrometer (Ocean Optics USB2000+, Orlando, FL, USA) with a deuterium and tungsten halogen light source (DH-2000). The transmittance and absorbance signals were traced under 190−800 nm spectra, and the medium of air was chosen as a reference background.

The orientation of the CNC particles in the films before and after ion-exchange modification was investigated with a polarized light microscope (PLM) (AmScope ME520TA, Irvine, CA, USA). A lambda (full wave) filter (530 nm), as a retardation plate to enhance the birefringence, was added between the halogen bulb and the sample. Images of −45 and +45° angles under the polarized light were collected and processed by ImageJ to extract the values from the blue channel of the RGB images. The birefringence orientation index (BOI) is calculated according to the following equation:[39]

$$\mathrm{BOI} = \frac{b_{-45^\circ} - b_{+45^\circ}}{b_{-45^\circ} + b_{+45^\circ}} \quad (1)$$

where b_{-45} and b_{+45} are the values of the blue channel for a pair of pixels in each image corresponding to the same voxel of the imaged material. Blue channel intensity could be selected for orientation because CNMs display birefringence color changing from blueish to yellowish between the two angles with retardation. BOI ranges from −1 to +1 where zero represents no orientation, while the +1 value represents the CNCs aligned in the reference direction and −1 means alignment in the perpendicular direction.

Scanning Electron Microscopy. The morphology of CNC films was evaluated with a field-emission scanning electron microscope (FE-SEM). Before imaging, films were adhered to the stub via conductive tape and sputter-coated with a 2−3 nm thin layers of gold/palladium. FE-SEM was performed at a 4.0 mm working distance and 2.0 kV accelerating voltages (Zeiss NVision 40, Jena, Germany). Elemental distribution in the films was detected by using energy-dispersive X-ray spectroscopy (IXRF EDS, Austin, TX, USA). Cross sections of CNC films were fractured after soaking in liquid nitrogen.

Barrier Properties of Films. The water vapor transmission rates (WVTRs) of films were measured and calculated according to the ASTM E96/E96M-16 standard. Around 7 cm diameter circles were obtained by cutting the edges from the conditioned films. A circular sample was placed on top of a Mason jar with 50 g of distilled water inside and sealed tightly with a silicone rubber gasket and a metal screw cap. The amount of water in the jar gave a distance of 19 mm between the surface and the sample. The jars were placed in a conditioning room (23 °C and 50% RH), and weight changes were recorded on 1, 2, 3, 5, and 7 days to calculate WVTRs using the following equation:

$$\mathrm{WVTR} = G/tA \quad (2)$$

where G is the weight change (g), t is the time (day), A is the test area of the film (m^2), and (G/t) is the slope of the straight line of the weight change against time. Three film replicates were tested.

The oxygen barrier properties of CNC films were evaluated by measuring oxygen transmission rate (OTR) values. An oxygen permeation analyzer (MOCON OX-TRAN 2/22, Minneapolis, MN, USA) was used for OTR measurement based on the ASTM F1927 standard. Samples were stored under the same condition with the testing (23 °C, 50, or 85% RH) until reaching the equilibrium state

https://doi.org/10.1021/acssuschemeng.2c01805
ACS Sustainable Chem. Eng. 2022, 10, 9419−9430

before the measurement. Within testing, at least 5 testing cycles were run and testing was terminated when the variation between two consecutive measurements was smaller than 1%.

Oil barrier property is another important factor of films that needs to be evaluated for food packaging application, which could be determined by an oil resistance test. The testing procedure was according to the TAPPI T559 pm-96 standard. A series of reagents mixed by different ratios of castor oil, toluene, and *n*-heptane (Kit No. 1-12) were dropped on the film surface from 13 mm height and removed after 15 s. The highest kit No. without darkening the test specimen was reported as the oil/grease performance test result.

Flame Retardancy of CNC Films. Approximately 3 × 1 cm^2 rectangular shape films were cut for flammability testing. The specimens were held vertically with a tweezer and exposed to a flame. After ignition, the flame was removed from films immediately, and the combustion images and time were recorded. The flammability test was operated according to the method used by Sakuma et al.[40]

Mechanical Properties of CNC Films. The tensile strengths, elastic moduli, and elongation at break of CNC films were determined using an Instron 5966 (Instron, Norwood, MA, USA) with 500 N load capacity. Dog-bone shape specimens with 10 mm width in the middle part were cut from films and conditioned at 23 °C and 50% RH before testing. The crosshead speed was 1 mm/min, and at least six replicates were run for average result calculation.

The test results were statistically analyzed with an IBM SPSS V28 (IBM Corp., Armonk, NY, USA). The differences among the group means were determined by one-way analysis of variance (ANOVA), and the means were statistically grouped via Duncan's multiple-range test based on a 95% confidence level.

RESULTS AND DISCUSSION

Characterization of CNC Suspensions. It was observed that hydrogels formed rapidly when the metal cations were added and diffused into the CNC suspensions, which is similar to what was reported in previous studies with TEMPO-CNF treatment by metal ions.[41,42] However, the purpose of adding metal cation solutions into CNC suspensions in this study was to ion-exchange the Na^+ on the CNC surface not to maintain the hydrogel state; in order to promote trivalent ion attachment with the sulfate half-ester groups on the CNC surface and replace the Na^+ ion, the hydrogels were stirred continuously for 2 h and formed a viscous liquid. Figure 3a shows the CNC suspensions with Fe^{3+} and Al^{3+} exchange visually. The Fe^{3+}-exchanged suspensions were yellow, and the Al^{3+} exchange led to a milky white color. CNC suspensions treated with low concentrations of Fe^{3+} or Al^{3+} displayed lighter color and lower turbidity or even a semitransparent state for Fe^{3+} compared with medium and high ion concentrations. However, there was no significant color difference of CNC suspensions observed between medium and high ion strength modification.

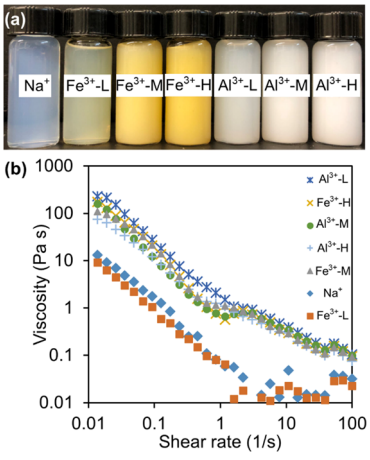

Figure 3. (a) Photographs and (b) viscosity behavior of CNC suspensions before and after ion-exchange modification.

This is consistent with steady-state shear viscosity performance (Figure 3b). The initial viscosity of the original CNC suspension (Na^+) was around 10 Pa·s, and CNCs with low-concentration Fe^{3+} treatment produced similar viscosity data. Other ion-exchanged CNC suspensions showed higher initial viscosity, around 100 Pa·s, which indicates more than a factor of 10 increase. All suspensions exhibited a typical shear thinning behavior, but these five groups could still have a viscosity of about 0.1 Pa·s at a 100 s^{-1} shear rate; however, the viscosity of CNC-Na and CNC-Fe-L was significantly reduced to about 0.01 Pa·s only at 4 s^{-1}. From the ICP results (Table 1), it was observed that the Na^+ content decreased from 387 mmol kg^{-1} to 77 and 76 mmol kg^{-1}, respectively, after Fe-M or Al-M treatment and to 53 and 44 mmol kg^{-1}, respectively, with Fe-H or Al-H modification. This result suggests a successful ion-exchange process, most Na^+ could be replaced by trivalent ions, and medium-concentration modification was more efficient. Meanwhile, the significant changes in the turbidity and viscosity of ion-exchanged CNC suspensions indicated that cross-linking among CNCs was formed by trivalent metal ions interacting with hydroxyl groups by the ligand[43] or sulfate half-ester groups on the CNC surface, while monovalent sodium ions are usually dissociated with sulfate groups and hydrated in water. Moreover, the CNC particles with low-concentration Fe^{3+} treatment could not be precipitated by 5000 rpm and 10 min centrifugation (Figure S1). The difference in suspension performance between Fe-L- and Al-L-modified CNCs after centrifugal washing shows that Al^{3+} had a better capability in creating ionic cross-linking than Fe^{3+} at low ionic concentrations. This is probably because the ion radius of Al^{3+} is smaller than that of Fe^{3+}, resulting in a strong and stable interaction.[44] Meanwhile, the high metal ion concentration at a metal ion to sulfate ratio of 3:1 did not induce further viscosity increases than the medium metal ion concentration because the content of sulfate ions on the CNC surface was limited (387 mmol kg^{-1}). Namely, a medium metal cation concentration probably consumed most of the available sulfate.

TEM images (Figure 4a,b) clearly show CNC morphology after negative staining similar to those reported in previous studies.[13,45] Although hydroxyl groups on the CNC surface led to hydrogen bonding and resulted in several CNCs aligning together, the repulsive force among Cell-OSO_3^- and Na^+ contributes to the uniform and random distribution of the CNCs in general. In contrast, trivalent metal cations, Fe^{3+} and Al^{3+}, resulted in a cross-linked CNC structure, except for Fe-L-modified CNCs. As shown in Figure 4d–h, CNC particles were not separated alone; instead, they showed a strong association with each other. Besides, the interconnection between metal ions and the CNCs was slightly enhanced under higher concentrations from the ion-exchange treatment but not significantly. This performance is consistent with the above visual characterization and viscosity tendency.

Here, the effect of the trivalent ions $Fe^{3+}$and Al^{3+} on sulfate anions on the CNC was observed as shown in Figure 4: sulfate anions on cellulose (Cell-OSO_3^-) interact with the metal ions, leading to the change of the structure of the suspension from the colloid (Figure 4a,c) to gel (Figure 4e,f) to loose

https://doi.org/10.1021/acssuschemeng.2c01805
ACS Sustainable Chem. Eng. 2022, 10, 9419−9430

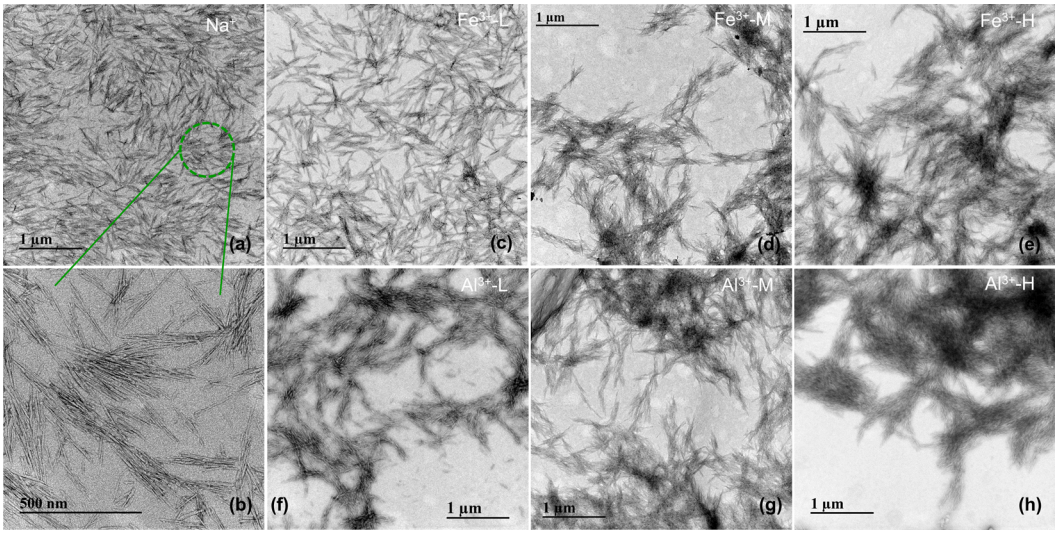

Figure 4. TEM images of the (a,b) original CNCs and ion exchange with (c) Fe-L, (d) Fe-M, (e) Fe-H, (f) Al-L, (g) Al-M, and (h) Al-H.

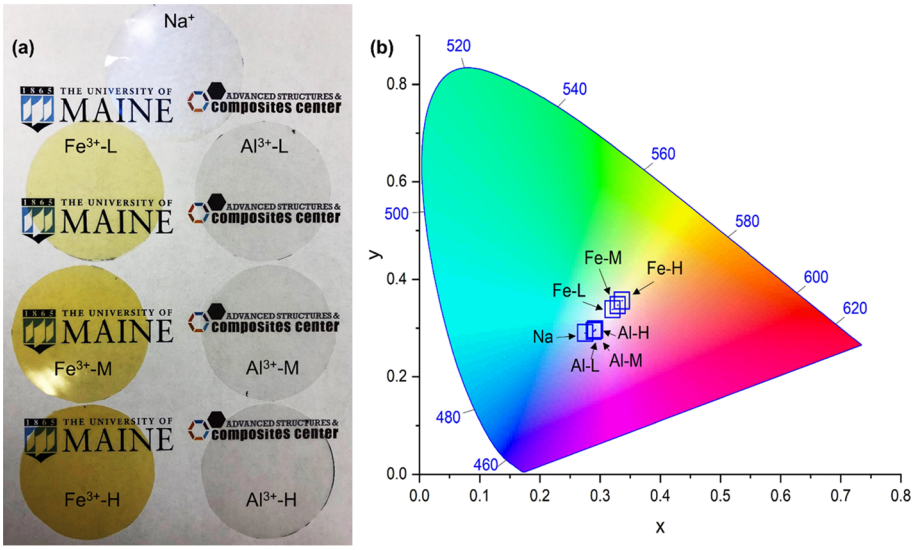

Figure 5. (a) Photo of CNC films and their (b) chromaticity diagram. University of Maine and Advanced Structures and Composites Center grant permission to use the logos in this figure.

agglomerates (Figure 4g,h) to a degree depending on both the concentration and complexing capability of metal ions. The viscosity of the suspension would increase from the colloidal to gel state but would decrease after further agglomeration and consolidation. The viscosity data as shown in Figure 3b are well in agreement with the state of crosslinks as shown in Figure 4. It is speculated that the complexing capability of Fe^{3+} is lower than that of Al^{3+}. Within the investigated concentrations of Fe^{3+}, the viscosity increases with the Fe^{3+} concentration. However, with a stronger capability, a low concentration of Al^{3+} achieves a similar effect to a high concentration of Fe^{3+}, resulting in the highest viscosity, and the higher concentrations of Al^{3+} result in agglomeration and consolidation decreasing the viscosity.

Physical Properties of the CNC Films. The CNC film without any plasticizer was too brittle to be peeled off from the Petri dish after casting (Figure S3a), and the mechanical properties could not be tested. However, flexible films could be easily obtained by adding 15 wt% sorbitol to the CNC (Figure S3b–d), which is the optimal amount for CNC film fabrication according to the mechanical properties.[46] Meanwhile, high-performance and free-standing CNC films with Fe^{3+} and Al^{3+} ion-exchange treatments by different cation concentrations were prepared. As shown in Figure 5a, the logos (Advanced Structures and Composites Center at the University of Maine) under the films are very clear, which reflects the high optical transparency with all formulation treatments. The quantitative color value of the films was evaluated using a chromaticity diagram (Figure 5b). The CNC-Na film is transparent with just a hint of light blue color. The rod-shaped chiral nematic crystal structures with a left-handed helical orientation of CNCs in aqueous suspensions were preserved in the film when water was evaporated completely.[47] An iridescent color appeared in the CNC film mainly owing to certain wavelengths of visible light being reflected from the helical pitch structure.[48] Blue color is always associated with a narrow pitch,[49,50] which was verified from the denser films that were fabricated (Figure S2). CNC-Fe films exhibited a yellow color attributed to Fe^{3+} and became darker with higher ion exchange modification. The color of CNC-Al films was close to white, and there was no

https://doi.org/10.1021/acssuschemeng.2c01805
ACS Sustainable Chem. Eng. 2022, 10, 9419−9430

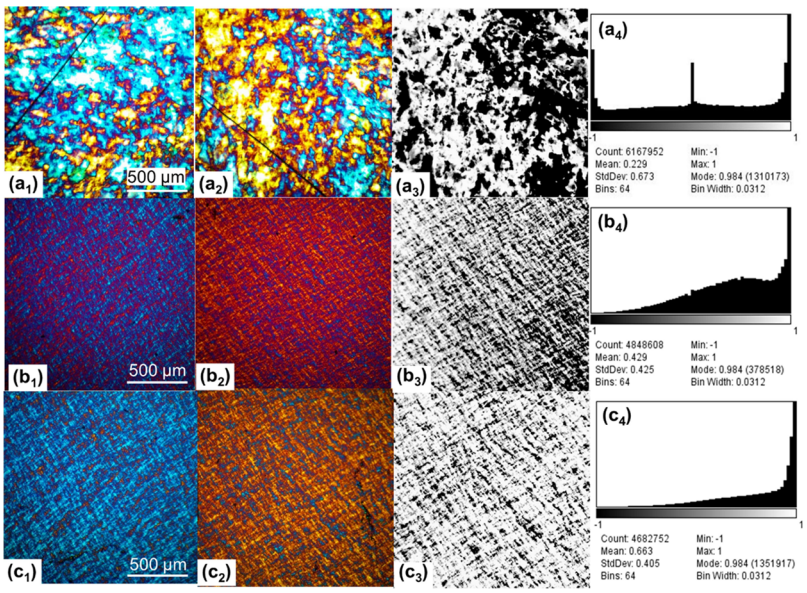

Figure 6. Images obtained at −45° (1) and +45° (2) angles by PLM, BOI ImageJ images (3), and BOI distribution (4) of (a) CNC-Na^+, (b) Fe^{3+}-M, and (c) Al^{3+}-M films.

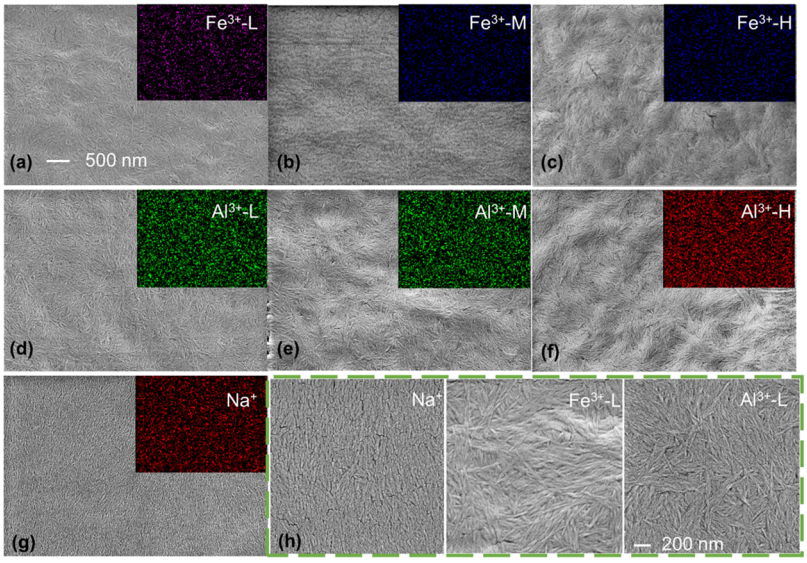

Figure 7. Surface morphology and elemental distribution of the CNC films: (a) Fe^{3+}-L, (b) Fe^{3+}-M, (c) Fe^{3+}-H, (d) Al^{3+}-L, (e) Al^{3+}-M, (f) Al^{3+}-H, and (g) Na^+, with the 500 nm scale bar for all images; (h) higher magnification images for the film surface, with the 200 nm scale bar for the three images.

drastic difference among the three cation concentrations evaluated.

The thickness of the CNC-Na films was 32 μm (Figure S2) at a target weight of 40 g/m^2. The other CNC-Fe and CNC-Al films were prepared according to the recalculated solids' weight content after the ion-exchange process and washing. Although they showed minor deviations of the thickness, varying from 33 to 36 μm, there was no significant statistical difference among them or compared with the CNC-Na film. For the density, CNC-Na films had similar results (1.6 g/m^3) to the previous studies,[16] and medium- and high-concentration Fe^{3+} and Al^{3+} ion-exchanged films did not exhibit significant decreases. However, neither low-concentration Fe^{3+} nor Al^{3+} ion modification reduced the density of CNC films to 1.45 g/m^3 (density of the self-organized CNC film reported by Shrestha et al.[51]). It was demonstrated that metal ions changed the CNC particles aligned way from the chiral nematic structure to the cross-linked structure during film production, but the films would retain their density as long as reaching a certain ion concentration, which is important for the properties of CNC films.

CNCs can spontaneously organize into a chiral nematic structure with left-handed helical orientation above the critical concentration. Such fascinating character is preserved in solid films after water evaporation as mentioned earlier.[48,50,52] In this study, metal ions can promote crosslinking, which could probably change the typical structure of CNC films. Thus, PLM as a facile method to identify the orientation of birefringent materials with the assistance of a lambda filter[39,52,53] was used for reflecting the structure difference between CNC-Na and ion-exchanged films. CNMs show dark and bright areas under PLM and shift to blue and yellow color

https://doi.org/10.1021/acssuschemeng.2c01805
ACS Sustainable Chem. Eng. 2022, 10, 9419−9430

with a retardation plate. This bluish and yellowish birefringence color changed when rotating the samples.[39,54] This is presented in Figure 6a$_{1-2}$; the blue and yellow color areas completely reverse in the −45° and +45° images for CNC-Na films. However, the ion-exchanged films resulted in a different orientation structure. Large areas of blue and yellow color intermixed together in the CNC-Na film, but one color is dominant in the Fe^{3+} and Al^{3+} ion-modified films. This could be described quantitatively by BOI, and results are shown in Figure 6a$_4$−c$_4$. For the original CNC-Na film, the average orientation BOI value was 0.23, between the 0 of perfect isotropic materials and 0.5 of CNF films.[39] Rather, the BOI value of CNC-Fe and -Al films increased to 0.43 and 0.66, respectively. This demonstrates that exchanging monovalent ions with trivalent ions into CNCs changed the chiral nematic behavior of CNC films and led nanocrystals to a higher extent of orientation. In addition, the modification efficacy of Al^{3+} was better than that of Fe^{3+}. The more detailed structure of films will be shown in SEM images.

The out-of-order CNC suspensions formed dense and high-quality CNC films by casting fabrication (Figure S4). The morphology of CNC film surfaces was drastically changed by different concentrations of Fe^{3+} and Al^{3+} modification, which is evident in the FE-SEM images (Figure 7). Cellulose crystals in the CNC-Na film displayed chiral nematic alignment arrangement (Figure S4b), while the metal cations caused them to reassemble and led to form a circle-shaped arrangement by ion cross-linking effect (Figures 7a−f and S5). Theoretically, one highly charged metal cation (Fe^{3+} or Al^{3+}) should connect with three sulfate half-ester groups on different CNC rods (Figure 2); namely, cross-linking reaction among cellulose crystals occurred in suspension, accompanied by a circle-shaped structure observed on films after water evaporation. Additionally, all images were collected under the same magnification, but cellulose crystals in the ion-exchanged films were clearer and easier to observe compared to the CNC-Na film. This phenomenon is related to a larger size formation, which could further verify CNC cross-linking and recombination after metal ion modification. The morphology changes could also be observed from cross-sectional SEM images (Figure S6), and the typical chiral nematic arrangement of the CNC structure with a clear pitch length disappeared in the Fe^{3+} and Al^{3+} ion-exchanged films.

Sodium (Figure 7g), ferric (Figure 7a−c), or aluminum (Figure 7d−f) ion distribution maps were obtained by SEM-EDS. Each type of ion in the films showed uniform distribution by fluorescence color dots displayed on the black background. The Fe^{3+} and Al^{3+} distribution status was similar to that of Na^+ in the CNC films before ion-exchange treatment, which demonstrated that the metal cations were added to the CNCs successfully by the ion-exchange method.

UV-Shielding Properties of CNC Films. UV light is composed of UV-A (320−400 nm), UV-B (280−320 nm), and UV-C (200−280 nm),[55] which are common wavelengths produced by sunlight. Overexposure to UV radiation can accelerate the deterioration of organic packaging materials[56] and packaged food. Therefore, transparent films with a UV protection function for packaging applications are necessary. The UV shielding properties of the ion-treated CNC films were assessed with a UV−vis spectrometer. The transmittance and absorbance spectra of films in the region of 200−800 nm wavelength were collected (Figure 8). The CNC films exhibited sufficient UV-shielding performance with Fe^{3+}

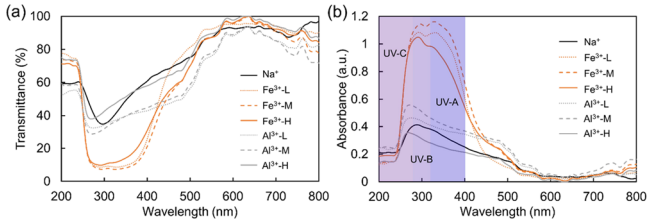

Figure 8. (a) UV−vis transmittance and (b) absorbance spectra of CNC films.

addition, where Fe-M ion-exchanged samples showed the highest UVA, UVB, and partially UVC absorption intensity (Figure 8b), almost three times higher than that of the unmodified film. In the transmittance curves, this was revealed by excellent UV shielding with a fairly low transmittance signal recorded in the region of 260−400 nm (Figure 8a). The UV absorption ability of Fe^{3+} is similar to that of the TEMPO-CNF films modified with Fe^{3+}, which displayed UV-absorbing ability.[32,33] Transmittance data could also be used to estimate the transparency of the CNC films under visible light wavelengths. The transmittance of all CNC films was higher than 95% at 600 nm except for Al-M and Al-H (89%). The slightly lower transmittance is probably attributed to the cross-linking and light scattering effects from the ions. However, generally, all films exhibited excellent transparency, which is consistent with the optical results in Figure 5a. In summary, CNC-Fe films achieved high visible light transparency with efficient UV blocking properties, simultaneously.

Barrier Properties of Films. For most packaging applications, the water vapor permeation property is an important index. The desirable WVTR value varies a few tenths to several thousand g m^{-2} day^{-1}, depending on the requirements of specific objects being packaged. Typically, the type of material, preparation method, and thickness of films are factors that influence WVTRs. In this research, the WVTR of the CNC-Na film was 557 g m^{-2} day^{-1} (Figure 9a), which is similar to results of Wang et al..[16] With the introduction of

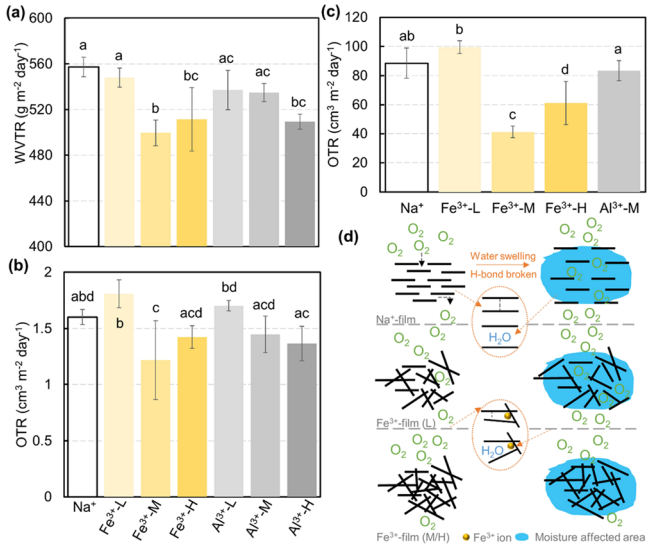

Figure 9. (a) WVTR of CNC films after 7-day equilibration and OTR value at 23 °C and (b) 50% and (c) 85% RH. The (d) diagram of O_2 transmission through CNC-Na, and CNC-Fe films under different RH.

https://doi.org/10.1021/acssuschemeng.2c01805
ACS Sustainable Chem. Eng. 2022, 10, 9419−9430

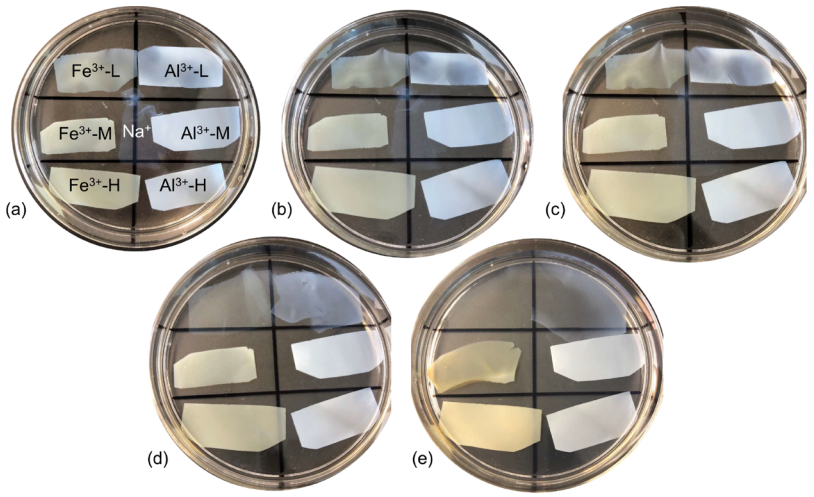

Figure 10. CNC films soaked in distilled water after (a) 0 min, (b) 5 min, (c) 1 h, (d) 3 h, and (e) 1 day.

metal cations, the WVTR of CNC films was reduced to between 500 and 547 g m^{-2} day^{-1}. Wherein, Fe^{3+} at a medium concentration produced films with the best moisture barrier performance (500 g m^{-2} day^{-1}), followed by Al^{3+} at high-concentration ion-exchange treatment (509 g m^{-2} day^{-1}). There are large amounts of hydroxyl groups on the CNC surface, and the film is formed through hydrogen bonding; however, hydrogen bonding is easily destroyed by water and more water molecules pass through. This situation could be partially improved by introducing metal cations into the CNC system because cross-linking still exists between the cation and sulfate half-easter group on the CNC when hydrogen bonding is destroyed. Therefore, they showed better moisture barrier properties.

Besides moisture, oxygen is directly related to food decay and spoilage caused by microorganisms. Thus, the oxygen barrier property is one of the essential requirements for adequate food packaging. All CNC films exhibited excellent oxygen barrier properties with only about 1.5 cm^3 m^{-2} day^{-1} OTR value at medium RH (50%). The high O_2-barrier performance of CNC films originates from the opposite polarity between hydroxyl groups on cellulose and oxygen molecules, strong hydrogen bonding among hydroxyls, and high film crystallinity[16] (Figure 9d). However, the barrier performance decreased dramatically with increasing RH above 50%. The OTR of the CNC-Na film increased to 88 cm^3 m^{-2} day^{-1} at 85% RH (Figure 9c), which can be classified as a "medium" grade oxygen barrier material. A slight increase in OTR was discovered after ion exchange with low-concentration metal cations. The low-dosage ion cross-linking occurring affected the original CNC self-assembly behavior and changed their microscopic morphology structure; namely, the CNC was not aligned as a chiral nematic structure, which was shown in the dense CNC film, but the cross-linking networks among CNCs formed by low concentration ions were not strong enough to prevent gas molecule transmission. In addition, low-concentration treatment led to lower density CNC films as well (Figure S2). When the ion concentration was increased to the medium level, the OTR of the CNC-Fe film decreased to 41 cm^3 m^{-2} day^{-1}, which is half the OTR of unmodified CNC films. The cross-linking among CNCs and ions ensured that certain barrier properties would be maintained after hydrogen bonding was disrupted by water molecules. With the increasing concentration, the advantage of cross-linking could not compensate for the adverse influence from structural changes on the OTR. Therefore, the medium ion-exchanged concentration is optimal, which can balance the effect from structural changes and cross-linking.

The oil/grease resistance results are displayed in Figure S7. The reagents (Kit No. 1-12) were prepared with various ratios of castor oil, toluene, and *n*-heptane to obtain different viscosities and surface tensions. The higher the kit no. measured from reagent testing, the better the oil barrier property the CNC film possesses. All CNC films (modified and unmodified samples) scored No.12 and showed excellent oil/grease resistance. In Figure S7, the reagents penetrated through the paper sample and left a stained area. As for the CNC films, the No. 12 reagent did not penetrate the film but rather stayed on the film surface, which remained clean after wiping off the reagent. High cohesive energy density,[57] a dense structure (low porosity), and impermeability against oil of crystalline are the primary reasons why CNC films have excellent oil barrier properties.[17,58,59] Interestingly, films with excellent oxygen barriers are usually accompanied by oil and grease hold-out.[60]

Water Resistance. In Figure 10, the CNC-Na film began to disintegrate immediately when put in water and entirely disintegrated within 5−10 min. The low-concentration-ion-treated films performed worse among the modified films, starting to lose integrity at 3 h and completely disintegrated in 1 day. The CNC films with medium- and high-concentration Fe^{3+} and Al^{3+} treatments exhibited durability after soaking in water where they retained a stable shape after 1 day. The water soaking experiment indicated that the CNC films with proper trivalent-ion-exchanged modification could improve the water durability significantly, which could be beneficial in wet packaging applications.

Flammability Tests. When a strip of the CNC-Na film was ignited from one end, the flame spread stably toward the other end until the strip burned out in 6 s (Figure 11). The trivalent-ion-modified films exhibited better self-extinguishing capabilities than the CNC-Na films whose extent depended on ion species and concentrations. The CNC-Fe films showed improved flame retardancy with the increasing concentration of Fe^{3+} (Figure 11). The CNC-Al films performed better than the CNC-Fe films in flame retardancy. The low-concentration

https://doi.org/10.1021/acssuschemeng.2c01805
ACS Sustainable Chem. Eng. 2022, 10, 9419−9430

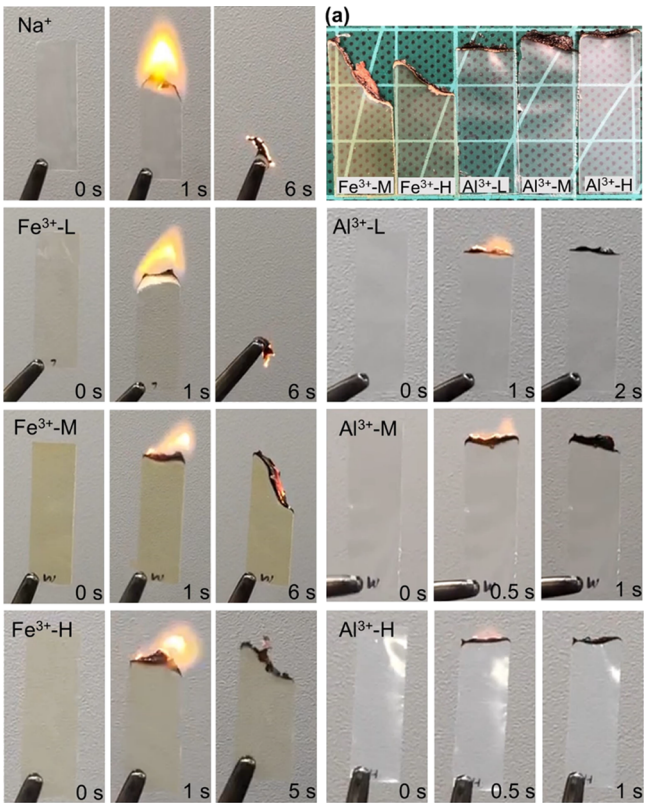

Figure 11. Flammability test results of the unmodified and modified CNC films and (a) films after testing.

Al^{3+} film extinguished the fire in 2 s, while the medium- and high-concentration films did it in less than 1 s and remained almost intact. The films after flammability testing are exhibited in Figure 11a, and Al^{3+} ion-exchanged films almost remained intact (3 cm of original sample size). The improved flame retardant property is probably attributable to the formation of hydrolyzed products of trivalent cations. The heat absorption lowers the temperature; the water vapor dilutes the combustible gases; the oxide forms a barrier layer. The combining effect of these three factors suppresses the burning of samples.[40,61,62]

Tensile Properties of CNC Films. As previously reported,[63,64] although neat CNC suspensions could form dense films after solvent evaporation, the films are too brittle to handle, and the same situation occurred here (Figure S3a). A limited amount of plasticizers, such as sorbitol, glycerol, or poly (vinyl alcohol), are usually introduced to address this shortcoming as demonstration.[46,64,65] Accordingly, CNC films were prepared with 15 wt% sorbitol content and showed flexible (Figure S3b–d) and better folding performance (Figure S8). The investigation of mechanical properties was also carried out. The tensile strength, Young's modulus, and elongation at break of the samples are shown in Figures 12 and S9, respectively. The original CNC-Na film had the best tested tensile properties with 48.9 MPa in strength, 8.1 GPa in Young's modulus, and 1.23% in elongation at break, which is much higher than those of previously reported pure CNC films without plasticizers with a tensile strength below 10 MPa, 0.9% in elongation at break, and 1.92 GPa in modulus.[66−68] After undergoing ion exchange via Fe^{3+} and Al^{3+}, there was a gradual decrease in tensile strength and elongation at break with an increase in ion concentration. This indicated that the tensile strength of the new morphological structures formed by trivalent ion cross-linking was not as high as the initial chiral nematic structure of the CNC-Na films. Despite this, all films showed excellent tensile properties with tensile strength and moduli above 38.9 MPa and 6.2 GPa, respectively. These tensile properties of CNC films are better than those of most nature-based films and comparable to those of some commercial plastic films, such as PE (7−31 MPa), PP (27−98 MPa), PS (31−49 MPa),[69] etc.

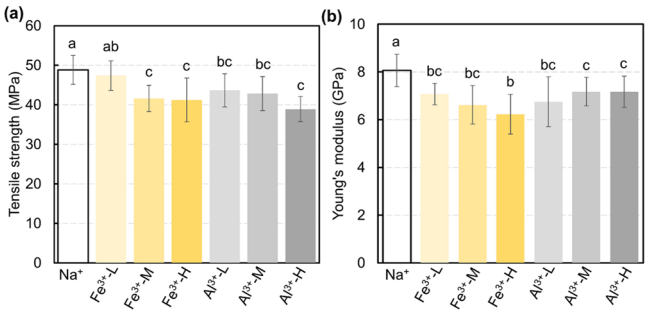

Figure 12. (a) Tensile strength and (b) modulus of CNC films with different ion modifications.

CONCLUSIONS

In this work, high-quality (flexible, free-standing, and high visible light transparency) CNC films were fabricated via metal cation ion-exchange treatment, followed by a solution casting method. $AlCl_3$ and $FeCl_3$ solutions with three different concentrations were used to evaluate the effect on the properties of CNC suspensions and films. The viscosity and turbidity of the CNC suspensions increased with ion addition, attributed to the successful cross-linking between ions and $-O-SO_3-$ groups on the CNC surface. The incorporation changed the appearance of CNC suspensions and films. For example, Fe^{3+} led to a yellow color. Meanwhile, Fe^{3+} contributed to the excellent UV-shielding performance of the films, where no significant difference between medium and high ion strength modification films was discovered. In addition, Fe^{3+} or Al^{3+} improved the moisture and oxygen barrier properties of the CNC films and imparted CNC films with durability in water. Moreover, the ion-exchanged films exhibited excellent fire self-extinguishment. The high transparency of the CNC films with multifunctional properties suggests great potential for next-generation packaging applications.

ASSOCIATED CONTENT

Supporting Information

The Supporting Information is available free of charge at https://pubs.acs.org/doi/10.1021/acssuschemeng.2c01805.

Additional experimental details and photos, density and thickness of films, SEM images, oil/grease resistance, and elongation at break results (PDF)

AUTHOR INFORMATION

Corresponding Authors

Jinwu Wang − *Forest Products Laboratory, U.S. Forest Service, Madison, Wisconsin 53726, United States;* orcid.org/0000-0002-8363-1689; Phone: (207) 307-6034; Email: jinwu.wang@usda.gov

https://doi.org/10.1021/acssuschemeng.2c01805
ACS Sustainable Chem. Eng. 2022, 10, 9419−9430

Douglas J. Gardner − *Advanced Structures and Composites Center, University of Maine, Orono, Maine 04469-5793, United States; School of Forest Resources, University of Maine, Orono, Maine 04469-5755, United States;* orcid.org/0000-0002-2903-2570; Phone: (207) 581-2846; Email: douglasg@maine.edu

Authors

Cong Chen − *Advanced Structures and Composites Center, University of Maine, Orono, Maine 04469-5793, United States; School of Forest Resources, University of Maine, Orono, Maine 04469-5755, United States;* orcid.org/0000-0003-0168-0709

Wenjing Sun − *School of Forest Resources, University of Maine, Orono, Maine 04469-5755, United States;* orcid.org/0000-0002-8850-6713

Lu Wang − *Advanced Structures and Composites Center, University of Maine, Orono, Maine 04469-5793, United States;* orcid.org/0000-0002-0458-8011

Mehdi Tajvidi − *Advanced Structures and Composites Center, University of Maine, Orono, Maine 04469-5793, United States; School of Forest Resources, University of Maine, Orono, Maine 04469-5755, United States;* orcid.org/0000-0002-3549-1220

Complete contact information is available at: https://pubs.acs.org/10.1021/acssuschemeng.2c01805

Author Contributions

C.C. designed and did the experiments and wrote the manuscript. W.S. designed and performed the fire-resistant experiment, performed data analysis, and did figure plotting. L.W. helped with film preparation and manuscript revision. M.T. helped with the analysis of data and edited the manuscript. J.W. conceived the general research, secured the funding, directed the research, and edited the text. D.J.G. conceived the general research, secured the funding, directed the research, and edited the text.

Notes

The authors declare no competing financial interest.

■ ACKNOWLEDGMENTS

This work was supported by the Agriculture and Food Research Initiative Foundational and Applied Science Program grant no. 2018-67010-27906 from the USDA National Institute of Food and Agriculture. The authors gratefully acknowledge the University of Maine Electron Microscope Laboratory for their support and assistance in this work.

■ REFERENCES

(1) Marsh, K.; Bugusu, B. Food packaging–roles, materials, and environmental issues. *J. Food Sci.* **2007**, *72*, R39−R55.

(2) Sangroniz, A.; Zhu, J. B.; Tang, X.; Etxeberria, A.; Chen, E. Y.; Sardon, H. Packaging materials with desired mechanical and barrier properties and full chemical recyclability. *Nat. Commun.* **2019**, *10*, 3559.

(3) Youssef, A. M.; El-Sayed, S. M. Bionanocomposites materials for food packaging applications: Concepts and future outlook. *Carbohydr. Polym.* **2018**, *193*, 19−27.

(4) PlasticsEurope; *Plastics—the Facts 2020*; PlasticsEurope, 2020.

(5) World Economic Forum; *The new plastics economy−rethinking the future of plastics*; Ellen MacArthur Foundation, McKinsey & Company, 2016.

(6) Raikova, S.; Knowles, T. D.; Allen, M. J.; Chuck, C. J. Co-liquefaction of macroalgae with common marine plastic pollutants. *ACS Sustainable Chem. Eng.* **2019**, *7*, 6769−6781.

(7) Helanto, K. E.; Matikainen, L.; Talja, R.; Rojas, O. J. Bio-based Polymers for Sustainable Packaging and Biobarriers: A Critical Review. *BioResources* **2019**, *14*, 4902−4951.

(8) Guillard, V.; Gaucel, S.; Fornaciari, C.; Angellier-Coussy, H.; Buche, P.; Gontard, N. The next generation of sustainable food packaging to preserve our environment in a circular economy context. *Front. nutr.* **2018**, *5*, 121.

(9) Rastogi, V. K.; Samyn, P. Bio-based coatings for paper applications. *Coatings* **2015**, *5*, 887−930.

(10) Chowdhury, R. A.; Nuruddin, M.; Clarkson, C.; Montes, F.; Howarter, J.; Youngblood, J. P. Cellulose Nanocrystal (CNC) Coatings with Controlled Anisotropy as High-Performance Gas Barrier Films. *ACS Appl. Mater. Interfaces* **2018**, *11*, 1376−1383.

(11) Wang, J.; Gardner, D. J.; Stark, N. M.; Bousfield, D. W.; Tajvidi, M.; Cai, Z. Moisture and Oxygen Barrier Properties of Cellulose Nanomaterial-Based Films. *ACS Sustainable Chem. Eng.* **2017**, *6*, 49−70.

(12) Trache, D.; Hussin, M. H.; Haafiz, M. K.; Thakur, V. K. Recent progress in cellulose nanocrystals: sources and production. *Nanoscale* **2017**, *9*, 1763−1786.

(13) Foster, E. J.; Moon, R. J.; Agarwal, U. P.; Bortner, M. J.; Bras, J.; Camarero-Espinosa, S.; Chan, K. J.; Clift, M. J. D.; Cranston, E. D.; Eichhorn, S. J.; Fox, D. M.; Hamad, W. Y.; Heux, L.; Jean, B.; Korey, M.; Nieh, W.; Ong, K. J.; Reid, M. S.; Renneckar, S.; Roberts, R.; Shatkin, J. A.; Simonsen, J.; Stinson-Bagby, K.; Wanasekara, N.; Youngblood, J. Current characterization methods for cellulose nanomaterials. *Chem. Soc. Rev.* **2018**, *47*, 2609−2679.

(14) Mu, R.; Hong, X.; Ni, Y.; Li, Y.; Pang, J.; Wang, Q.; Xiao, J.; Zheng, Y. Recent trends and applications of cellulose nanocrystals in food industry. *Trends Food Sci. Technol.* **2019**, *93*, 136−144.

(15) Tayeb, A. H.; Tajvidi, M. Sustainable Barrier System via Self-Assembly of Colloidal Montmorillonite and Cross-linking Resins on Nanocellulose Interfaces. *ACS Appl. Mater. Interfaces* **2019**, *11*, 1604−1615.

(16) Wang, L.; Chen, C.; Wang, J.; Gardner, D. J.; Tajvidi, M. Cellulose nanofibrils versus cellulose nanocrystals: Comparison of performance in flexible multilayer films for packaging applications. *Food Packag. Shelf Life* **2020**, *23*, No. 100464.

(17) Aulin, C.; Gällstedt, M.; Lindström, T. Oxygen and oil barrier properties of microfibrillated cellulose films and coatings. *Cellulose* **2010**, *17*, 559−574.

(18) Goodman, S. M.; Che, J.; Neri, W.; Yuan, J.; Dichiara, A. B. Water-processable cellulosic nanocomposites as green dielectric films for high-energy storage. *Energy Storage Mater.* **2022**, *48*, 497−506.

(19) Soni, B.; Hassan, E. B.; Schilling, M. W.; Mahmoud, B. Transparent bionanocomposite films based on chitosan and TEMPO-oxidized cellulose nanofibers with enhanced mechanical and barrier properties. *Carbohydr. Polym.* **2016**, *151*, 779−789.

(20) Isogai, A. Development of completely dispersed cellulose nanofibers. *Proc. Jpn. Acad., Ser. B* **2018**, *94*, 161−179.

(21) Kim, T.; Tran, T. H.; Hwang, S. Y.; Park, J.; Oh, D. X.; Kim, B.-S. Crab-on-a-tree: all biorenewable, optical and radio frequency transparent barrier nanocoating for food packaging. *ACS Nano* **2019**, *13*, 3796−3805.

(22) Reid, M. S.; Villalobos, M.; Cranston, E. D. Benchmarking Cellulose Nanocrystals: From the Laboratory to Industrial Production. *Langmuir* **2017**, *33*, 1583−1598.

(23) Wang, Q.; Zhu, J.; Reiner, R.; Verrill, S.; Baxa, U.; McNeil, S. Approaching zero cellulose loss in cellulose nanocrystal (CNC) production: recovery and characterization of cellulosic solid residues (CSR) and CNC. *Cellulose* **2012**, *19*, 2033−2047.

(24) Beck-Candanedo, S.; Roman, M.; Gray, D. G. Effect of reaction conditions on the properties and behavior of wood cellulose nanocrystal suspensions. *Biomacromolecules* **2005**, *6*, 1048−1054.

(25) Cheng, S.; Zhang, Y.; Cha, R.; Yang, J.; Jiang, X. Water-soluble nanocrystalline cellulose films with highly transparent and oxygen barrier properties. *Nanoscale* **2016**, *8*, 973−978.
(26) Gan, I.; Chow, W. Antimicrobial poly (lactic acid)/cellulose bionanocomposite for food packaging application: A review. *Food Packag. Shelf Life* **2018**, *17*, 150−161.
(27) Chaichi, M.; Hashemi, M.; Badii, F.; Mohammadi, A. Preparation and characterization of a novel bionanocomposite edible film based on pectin and crystalline nanocellulose. *Carbohydr. Polym.* **2017**, *157*, 167−175.
(28) Yadav, M.; Chiu, F. C. Cellulose nanocrystals reinforced kappa-carrageenan based UV resistant transparent bionanocomposite films for sustainable packaging applications. *Carbohydr. Polym.* **2019**, *211*, 181−194.
(29) Chowdhury, R. A.; Clarkson, C.; Apalangya, V. A.; Islam, S. M. N.; Youngblood, J. P. Roll-to-roll fabrication of cellulose nanocrystal-poly(vinyl alcohol) composite coatings with controlled anisotropy. *Cellulose* **2018**, *25*, 6547−6560.
(30) Nuruddin, M.; Chowdhury, R. A.; Szeto, R.; Howarter, J. A.; Erk, K. A.; Szczepanski, C. R.; Youngblood, J. P. Structure-Property Relationship of Cellulose Nanocrystal-Polyvinyl Alcohol Thin Films for High Barrier Coating Applications. *ACS Appl. Mater. Interfaces* **2021**, *13*, 12472−12482.
(31) Liu, R.; He, X.; Miao, M.; Cao, S.; Feng, X. In-situ growth of porous $Cu_3(BTC)_2$ on cellulose nanofibrils for ultra-low dielectric films with high flexibility. *J. Mater. Sci. Technol.* **2022**, *112*, 202−211.
(32) Yang, W.; Wang, X.; Gogoi, P.; Bian, H.; Dai, H. Highly transparent and thermally stable cellulose nanofibril films functionalized with colored metal ions for ultraviolet blocking activities. *Carbohydr. Polym.* **2019**, *213*, 10−16.
(33) Shimizu, M.; Saito, T.; Isogai, A. Water-resistant and high oxygen-barrier nanocellulose films with interfibrillar cross-linkages formed through multivalent metal ions. *J. Membr. Sci.* **2016**, *500*, 1−7.
(34) Reid, M. S.; Kedzior, S. A.; Villalobos, M.; Cranston, E. D. Effect of Ionic Strength and Surface Charge Density on the Kinetics of Cellulose Nanocrystal Thin Film Swelling. *Langmuir* **2017**, *33*, 7403−7411.
(35) Moud, A. A.; Arjmand, M.; Liu, J.; Yang, Y.; Sanati-Nezhad, A.; Hejazi, S. H. Cellulose nanocrystal structure in the presence of salts. *Cellulose* **2019**, *26*, 9387−9401.
(36) Metzger, C.; Auber, D.; Dähnhardt-Pfeiffer, S.; Briesen, H. Agglomeration of cellulose nanocrystals: the effect of secondary sulfates and their use in product separation. *Cellulose* **2020**, *27*, 9839−9851.
(37) 2020 Cellulose Lab Nanocellulose Products Price. https://www.cellulose lab.com/price/CelluloseLab%20Product%20Price%20List%202020.htm.
(38) Reiner, R. S.; Rudie, A. W. Process scale-up of cellulose nanocrystal production to 25 kg per batch at the forest products laboratory. In *Production and applications of Cellulose nanomaterials*; TAPPI Press, Chapter 1.1; 2013; Vol. *1*, pp 21−24.
(39) Ghasemi, S.; Rahimzadeh-Bajgiran, P.; Tajvidi, M.; Shaler, S. M. Birefringence-based orientation mapping of cellulose nanofibrils in thin films. *Cellulose* **2020**, *27*, 677−692.
(40) Sakuma, W.; Yamasaki, S.; Fujisawa, S.; Kodama, T.; Shiomi, J.; Kanamori, K.; Saito, T. Mechanically Strong, Scalable, Mesoporous Xerogels of Nanocellulose Featuring Light Permeability, Thermal Insulation, and Flame Self-Extinction. *ACS Nano* **2021**, *15*, 1436−1444.
(41) Dong, H.; Snyder, J. F.; Tran, D. T.; Leadore, J. L. Hydrogel, aerogel and film of cellulose nanofibrils functionalized with silver nanoparticles. *Carbohydr. Polym.* **2013**, *95*, 760−767.
(42) Zander, N. E.; Dong, H.; Steele, J.; Grant, J. T. Metal cation cross-linked nanocellulose hydrogels as tissue engineering substrates. *ACS Appl. Mater. Interfaces* **2014**, *6*, 18502−18510.
(43) Al-Sogair, F. M.; Operschall, B. P.; Sigel, A.; Sigel, H.; Schnabl, J.; Sigel, R. K. Probing the metal-ion-binding strength of the hydroxyl group. *Chem. Rev.* **2011**, *111*, 4964−5003.
(44) Benitez, A. J.; Walther, A. Counterion Size and Nature Control Structural and Mechanical Response in Cellulose Nanofibril Nanopapers. *Biomacromolecules* **2017**, *18*, 1642−1653.
(45) Chen, L.; Wang, Q.; Hirth, K.; Baez, C.; Agarwal, U. P.; Zhu, J. Tailoring the yield and characteristics of wood cellulose nanocrystals (CNC) using concentrated acid hydrolysis. *Cellulose* **2015**, *22*, 1753−1762.
(46) Csiszár, E.; Nagy, S. A comparative study on cellulose nanocrystals extracted from bleached cotton and flax and used for casting films with glycerol and sorbitol plasticisers. *Carbohydr. Polym.* **2017**, *174*, 740−749.
(47) Wang, P. X.; Hamad, W. Y.; MacLachlan, M. J. Structure and transformation of tactoids in cellulose nanocrystal suspensions. *Nat. Commun.* **2016**, *7*, 11515.
(48) Tran, A.; Boott, C. E.; MacLachlan, M. J. Understanding the Self-Assembly of Cellulose Nanocrystals-Toward Chiral Photonic Materials. *Adv. Mater.* **2020**, *32*, No. e1905876.
(49) Liu, D.; Wang, S.; Ma, Z.; Tian, D.; Gu, M.; Lin, F. Structure−color mechanism of iridescent cellulose nanocrystal films. *RSC Adv.* **2014**, *4*, 39322−39331.
(50) Tran, A.; Hamad, W. Y.; MacLachlan, M. J. Fabrication of Cellulose Nanocrystal Films through Differential Evaporation for Patterned Coatings. *ACS Appl. Nano Mater.* **2018**, *1*, 3098−3104.
(51) Shrestha, S.; Diaz, J. A.; Ghanbari, S.; Youngblood, J. P. Hygroscopic Swelling Determination of Cellulose Nanocrystal (CNC) Films by Polarized Light Microscopy Digital Image Correlation. *Biomacromolecules* **2017**, *18*, 1482−1490.
(52) Gray, D. G. Recent Advances in Chiral Nematic Structure and Iridescent Color of Cellulose Nanocrystal Films. *Nanomaterials (Basel)* **2016**, *6*, 213.
(53) Mashkour, M.; Kimura, T.; Kimura, F.; Mashkour, M.; Tajvidi, M. One-dimensional core−shell cellulose-akaganeite hybrid nanocrystals: synthesis, characterization, and magnetic field induced self-assembly. *RSC Adv.* **2014**, *4*, 52542−52549.
(54) Mashkour, M.; Kimura, T.; Kimura, F.; Mashkour, M.; Tajvidi, M. Tunable self-assembly of cellulose nanowhiskers and polyvinyl alcohol chains induced by surface tension torque. *Biomacromolecules* **2014**, *15*, 60−65.
(55) Gu, W.; Liu, X.; Li, F.; Shi, S. Q.; Xia, C.; Zhou, W.; Zhang, D.; Gong, S.; Li, J. Tough, strong, and biodegradable composite film with excellent UV barrier performance comprising soy protein isolate, hyperbranched polyester, and cardanol derivative. *Green Chem.* **2019**, *21*, 3651−3665.
(56) Parit, M.; Du, H.; Zhang, X.; Jiang, Z. Flexible, Transparent, UV-Protecting, Water-Resistant Nanocomposite Films Based on Polyvinyl Alcohol and Kraft Lignin-Grafted Cellulose Nanofibers. *ACS Appl. Polym. Mater.* **2022**, *4*, 3587−3597.
(57) Aulin, C.; Ström, G. Multilayered alkyd resin/nanocellulose coatings for use in renewable packaging solutions with a high level of moisture resistance. *Ind. Eng. Chem. Res.* **2013**, *52*, 2582−2589.
(58) Fein, K.; Bousfield, D. W.; Gramlich, W. M. Processing effects on structure, strength, and barrier properties of refiner-produced cellulose nanofibril layers. *ACS Appl. Polym. Mater.* **2021**, *3*, 3666−3678.
(59) Dai, L.; Long, Z.; Chen, J.; An, X.; Cheng, D.; Khan, A.; Ni, Y. Robust Guar Gum/Cellulose Nanofibrils Multilayer Films with Good Barrier Properties. *ACS Appl. Mater. Interfaces* **2017**, *9*, 5477−5485.
(60) Hubbe, M. A.; Ferrer, A.; Tyagi, P.; Yin, Y.; Salas, C.; Pal, L.; Rojas, O. J. Nanocellulose in thin films, coatings, and plies for packaging applications: A review. *BioResources* **2017**, *12*, 2143−2233.
(61) Witkowski, A.; Stec, A. A.; Hull, T. R. Thermal Decomposition of Polymeric Materials. In *SFPE Handbook of Fire Protection Engineering* Hurley, M. J.; Gottuk, D.; Hall, J. R.; Harada, K.; Kuligowski, E.; Puchovsky, M.; Torero, J.; Watts, J. M.; Wieczorek, C., Eds.; Springer New York: New York, 2016; pp 167−254.
(62) Yang, Z.; Li, H.; Niu, G.; Wang, J.; Zhu, D. Poly (vinylalcohol)/chitosan-based high-strength, fire-retardant and smoke-suppressant composite aerogels incorporating aluminum species via freeze drying. *Composites, Part B* **2021**, *219*, No. 108919.

(63) Wei, X.-Y.; Lin, T.; Wang, L.; Yin, X.-F. Effect of A Limited Amount of D-Sorbitol on Pitch and Mechanical Properties of Cellulose Nanocrystal Films. *Crystals* **2021**, *11*, 1324.
(64) Fernandez-Santos, J.; Valls, C.; Cusola, O.; Roncero, M. B. Improving Filmogenic and Barrier Properties of Nanocellulose Films by Addition of Biodegradable Plasticizers. *ACS Sustainable Chem. Eng.* **2021**, *9*, 9647−9660.
(65) Beck, S.; Bouchard, J.; Chauve, G.; Berry, R. Controlled production of patterns in iridescent solid films of cellulose nanocrystals. *Cellulose* **2013**, *20*, 1401−1411.
(66) Feng, K.; Dong, C.; Gao, Y.; Jin, Z. A Green and Iridescent Composite of Cellulose Nanocrystals with Wide Solvent Resistance and Strong Mechanical Properties. *ACS Sustainable Chem. Eng.* **2021**, *9*, 6764−6775.
(67) Sui, Y.; Li, X.; Chang, W.; Wan, H.; Li, W.; Yang, F.; Yu, Z. Z. Multi-responsive nanocomposite membranes of cellulose nanocrystals and poly(N-isopropyl acrylamide) with tunable chiral nematic structures. *Carbohydr. Polym.* **2020**, *232*, No. 115778.
(68) Hanif, Z.; Choi, D.; Tariq, M. Z.; La, M.; Park, S. J. Water-stable flexible nanocellulose chiral nematic films through acid vapor cross-linked glutaraldehyde for chiral nematic templating. *ACS Macro Lett.* **2020**, *9*, 146−151.
(69) Bastarrachea, L.; Dhawan, S.; Sablani, S. S. Engineering properties of polymeric-based antimicrobial films for food packaging: a review. *Food Eng. Rev.* **2011**, *3*, 79−93.

https://doi.org/10.1021/acssuschemeng.2c01805
ACS Sustainable Chem. Eng. 2022, 10, 9419−9430